Visible-light photocatalytic activity of Ni-doped TiO$_2$ from *ab initio* calculations

Yan-Ming Lin[a], Zhen-Yi Jiang[a,*], Chao-Yuan Zhu[b], Xiao-Yun Hu[c], Xiao-Dong Zhang[a], Jun Fan[d]

[a] *Institute of Modern Physics, Northwest University, Xi'an 710069, PR China*
[b] *Department of Applied Chemistry, Institute of Molecular Science and Center for Interdisciplinary Molecular Science, National Chiao-Tung University, Hsinchu 30050, Taiwan*
[c] *Department of Physics, Northwest University, Xi'an 710069, PR China*
[d] *School of Chemical Engineering, Northwest University, Xi'an 710069, PR China*

ARTICLE INFO

ABSTRACT

The geometrical structures and electronic properties of Ni-doped anatase and rutile TiO$_2$ were successfully calculated and simulated by a plane wave pseudopotential method based on density functional theory (DFT). Our results show that most Ni 3d states are located in the forbidden band of substitutional Ni to O-doped anatase and rutile TiO$_2$, and mix with O 2p states, resulting in a decrease of the photon excitation energy and red-shift of absorption edge compared to pure anatase and rutile. For substitutional Ni to Ti-doped anatase TiO$_2$ under O-rich growth condition, the band gap has a slight decline of about 0.05 eV compared with pure anatase TiO$_2$ and contains a series of impurity energy levels, which may be responsible for the experimental photocatalytic activity and red-shift of absorption edge.

1. Introduction

Titanium dioxide (TiO$_2$) has received much attention as a well-known photocatalytic material for the photogeneration of hydrogen from water and the remediation of organic pollutants [1,2]. However, a large intrinsic band gap of TiO$_2$ (3.2 eV for anatase structure [3] and 3.0 eV for rutile structure [1]) allows only a small portion of solar spectrum in the ultraviolet (UV) light region to be absorbed. Therefore, one of the major goals in photochemical applications is to improve the photocatalytic efficiency of TiO$_2$ under visible-light. It has been suggested that transition metal ions doped TiO$_2$ could realize visible-light absorption and impurity levels in the forbidden band of TiO$_2$ produced by transition metal ions were responsible for the visible-light absorption [4–6].

In recent years, Jin et al. [7] reported that the photocatalytic activity of Si-doped TiO$_2$ prepared *via* hydrothermal process is higher than that of Degussa P25 and pure TiO$_2$. Yang et al. [8], Shi et al. [9] studied the electronic properties of Si-doped and Si/N-codoped TiO$_2$, respectively. Sakthivel et al. [10], Li et al. [11], Choi et al. [12], Khan et al. [13], Wu et al. [14], Hsu et al. [15], and Irie et al. [16] also observed lower band gap energy and visible-light absorption of C-doped TiO$_2$. Zhao et al.'s report showed that incorporation of B into TiO$_2$ could extend the spectral response to the visible region and the photocatalytic activity is greatly enhanced as it is further loaded with Ni$_2$O$_3$ [17]. In addition, some researchers have made an attempt to improve the photocatalytic activity of TiO$_2$ and extend its optical absorption to the visible-light region by doping with Ni [18]. For example, Tseng et al. [19] studied the degradation of xylene vapor over Ni-doped TiO$_2$ photocatalysts prepared by polyol-mediated synthesis, and found that the photocatalytic activity of TiO$_2$ doped with appropriate content of Ni^{2+} exceeded that of P25 under UV light irradiation. Nakhate et al. [20] also observed that Ni-doped TiO$_2$ catalyst exhibits 63% more efficiency than undoped nanosize TiO$_2$ to degradation of methylene blue under visible-light irradiation, and found that Ni-doped TiO$_2$ shows red-shift to 550 nm which is due to Ni doping of rutile TiO$_2$. However, to the best of our knowledge, there have been few reports regarding the Ni doping effects on the electronic structures and optical properties of TiO$_2$ to reveal the physical and chemical origin of the enhanced photocatalytic activity and the longer wavelength optical absorption.

In this study, we performed density functional theory (DFT) calculations for the geometrical structures and the electronic properties of substitutionally Ni-doped anatase and rutile TiO$_2$ systematically. Our theoretical analysis provided a possible

* Corresponding author. Tel.: +86 29 88303491; fax: +86 29 88302331.
E-mail addresses: jiangzy@nwu.edu.cn, jiang_zhenyi@hotmail.com, linymnwu@gmail.com (Z.-Y. Jiang), hxy3275@nwu.edu.cn (X.-Y. Hu).
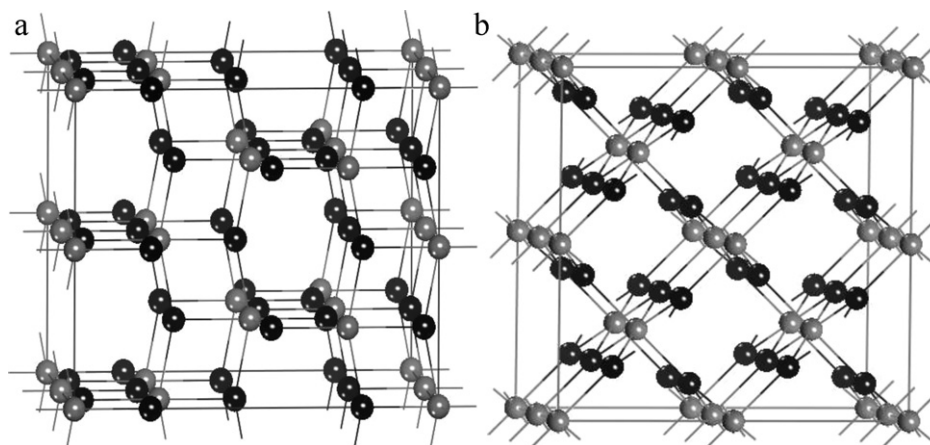
Fig. 1. (a) Anatase supercell ($Ti_{16}O_{32}$) and (b) rutile supercell ($Ti_{16}O_{32}$). Titanium atoms are gray spheres and oxygen atoms are black spheres.

explanation for experimentally observed optical absorption broadening to visible-light in Ni-doped TiO_2, and the thermodynamical properties of two possible Ni-doped TiO_2 modes are also discussed by calculating the formation energies of the substitutional defects.

2. Computational details

Crystallographic lattice of anatase and rutile TiO_2 belong to the $I4_1/amd$ and $P4_2/mnm$ tetragonal space group, respectively. We simulated Ni doping effects using $2 \times 2 \times 1$ (48-atom) repetition of the unit anatase and $2 \times 2 \times 2$ (48-atom) rutile TiO_2 supercell (see Fig. 1). Two possible Ni-doped anatase and rutile TiO_2 structures were considered by replacing an oxygen or titanium atom in the lattice with a nickel atom, such as substitutional Ni at the O site (Ni@O) and substitutional Ni at the Ti site (Ni@Ti) for the doped systems. The partial geometries taken from the structurally optimized Ni-doped anatase and rutile TiO_2 supercell are shown in Fig. 2.

All of the calculations were performed with the Vienna *ab initio* Simulation Package (VASP) code based on first-principles density functional theory [21]. The Perdew–Burke–Ernzerhof (PBE) parameterization [23] of the generalized gradient approximation (GGA) [22] was adopted for the exchange-correlation potential. The valence states are 2s and 2p shells for O with 6 valence electrons and 3s, 3p, 3d, and 4s states for Ti with 12 valence electrons. The Monkhorst–Pack [24] grid with $5 \times 5 \times 5$ k-points was used for integration in the Brillouin zone of the supercell, and the wave functions are expanded with the cutoff energy of 500 eV. Geometry optimization was carried out before static calculation. The convergence threshold of the self-consistent energy error is 10^{-5} eV and atomic relaxations were carried out until all components of the residual forces were less than 10^{-3} eV Å^{-1}.

The calculated crystal parameters of pure anatase and rutile TiO_2 model are $a = b = 3.788$ Å, $c = 9.497$ Å and $a = b = 4.595$ Å, $c = 2.957$ Å, which are in good agreement with the experiment values of $a = b = 3.782$ Å, $c = 9.502$ Å and $a = b = 4.593$ Å, $c = 2.959$ Å within 0.16%, respectively [25,26]. These results indicate that our

calculation methods are reasonable, and the calculated results are authentic.

3. Results and discussion

3.1. Defect formation energies

To probe the relative stability of two substitutional Ni-doped structures, we calculated the formation energies (E_f) for the two doping cases. The formation energies of substitutional Ni to O model and substitutional Ni to Ti-doped model are calculated according to the following formula

$$E_{f(Ni@X)} = E_{(Ni@X)} - E_{(pure)} - (\mu_{Ni} - \mu_X) \quad (X = O, Ti)$$

where $E_{(Ni@X)}$ and $E_{(pure)}$ are the total energies of Ni-doped and pure TiO_2 supercell, respectively. It should be noted that the formation energy depends on growth conditions, which may be either O- or Ti-rich. For TiO_2, the chemical potentials of O and Ti satisfy the relationship $\mu_{Ti} + 2\mu_O = \mu_{TiO_2}$, $\mu_O \leqslant \mu_{O_2}/2$, and $\mu_{Ti} \leqslant \mu_{Ti}^{metal}$. The chemical potential μ_O is determined by the energy of an O_2 molecule in the O-rich growth condition (corresponding to a high value of μ_O). By referencing μ_O to the energy of an O atom in the O_2 molecule, μ_{Ti} in the Ti-rich condition (corresponding to a high value of μ_{Ti}) amounts to the energy of one Ti atom in bulk Ti. μ_{Ni} is the chemical potential of Ni impurity, which is calculated from bulk nickel.

In the experiments [19,20], nickel is doped in the form of Ni^{2+} ion in Ni-doped TiO_2. Therefore, the Ni impurity in the form of Ni^{2+} ion is incorporated into the crystal of TiO_2 in our theoretical calculation. Our calculations show that the defect formation energies for Ni substitution depend on the growth conditions. The calculated formation energies in Ni-doped anatase and rutile TiO_2 were listed in Table 1. It can be observed that the formation energy of Ni@O is smaller than that of Ni@Ti under Ti-rich growth condition in Ni-doped anatase TiO_2 structure, and the formation energy of Ni@O is higher than that of Ni@Ti under the O-rich growth
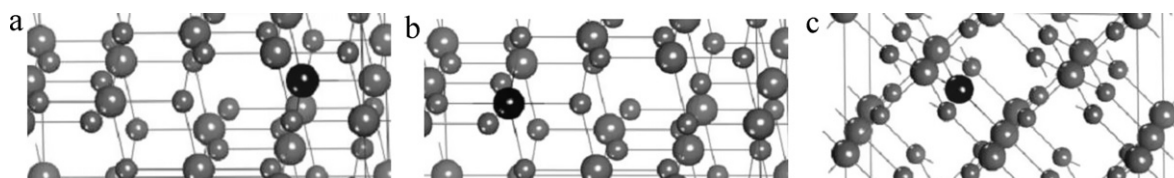

Fig. 2. Partial geometries for (a) Ni-doped anatase TiO_2 (Ni@O), (b) Ni-doped anatase TiO_2 (Ni@Ti), and (c) Ni-doped rutile TiO_2 (Ni@O). The big gray spheres represent titanium (Ti) atoms, the small gray spheres represent oxygen (O) atoms, and the big black spheres represent nickel (Ni) atoms.

Table 1
Calculated defect formation energies of Ni-doped anatase and rutile TiO_2 models (in eV).

Doped models	Defect formation energy (eV)	
	Ti-rich	O-rich
Anatase		
Ni@O	2.6591	8.0688
Ni@Ti	8.0914	−2.7280
Rutile		
Ni@O	5.3030	−5.5163
Ni@Ti	7.5789	−3.2404

The error range is 10^{-5} eV.

condition. The calculated results suggest easier replacement of O atom with Ni atom under Ti-rich growth condition, replacement of Ti atom with Ni atom under O-rich growth condition. In particular, under the O-rich growth condition, the formation energy of

Ni@Ti is negative, indicating that the Ni^{2+} impurity is readily incorporated into the crystal, partial geometries are shown in Fig. 2(a and b). For Ni-doped rutile TiO_2, our calculations suggest that the formation energy of Ni@O is smaller than that of Ni@Ti under both Ti-rich and O-rich growth conditions, this theoretical result indicates that Ni^{2+} impurity is preferred to substitute the O atom under both Ti-rich and O-rich growth conditions, partial geometry is shown in Fig. 2(c). Replacing an O or Ti atom with an Ni atom in anatase and rutile TiO_2 supercells results in significant local structural changing because Ni (0.69 Å) has a smaller ionic radius than O (1.4 Å) ion and a larger ionic radius than Ti (0.61 Å) ion. The results show that Ni-doped anatase and rutile TiO_2 leads to a significant lattice deformation, which changes the charge distribution pattern and the dipole moments, making a vacancy created nearby and the separation of photo-excited electron–hole pairs easier.
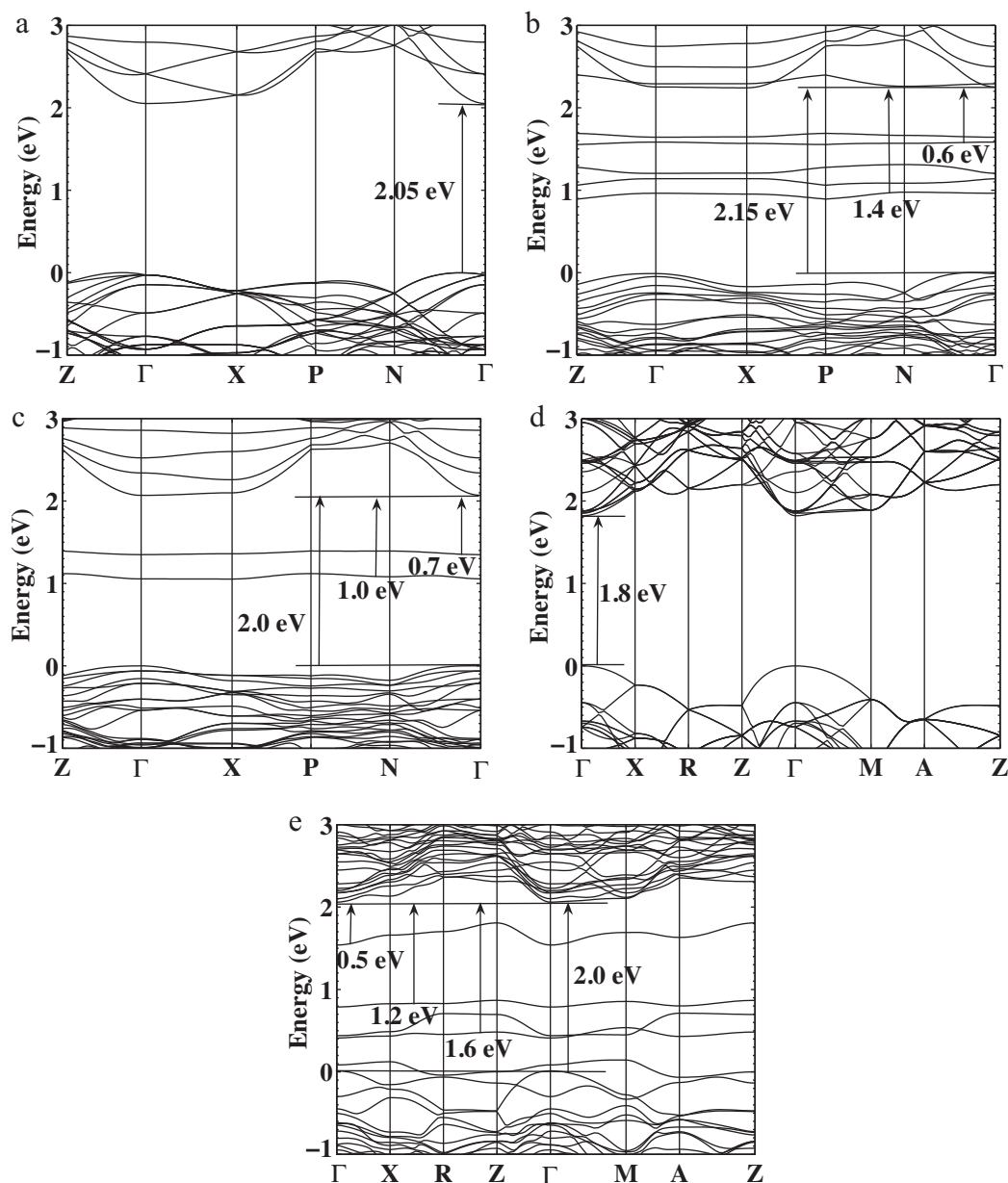

Fig. 3. Band structures for (a) pure anatase TiO_2, (b) Ni-doped anatase (Ni@O), (c) Ni-doped anatase (Ni@Ti), (d) pure rutile TiO_2, and (e) Ni-doped rutile (Ni@O). The top of the valence band of pure anatase and rutile TiO_2 are taken as the reference level. X-axis is high symmetry k points of the first Brillouin zone. For anatase, Γ(0, 0, 0), N(0,1/2,0), X(0,0,1/2), Z(1/2,1/2,-1/2), and P(1/4,1/4,1/4). For rutile, Γ(0, 0, 0), M(1/2,1/2,0), Z(0,0,1/2), A(1/2,1/2,1/2), R(0,1/2,1/2), and X(0,1/2,0).

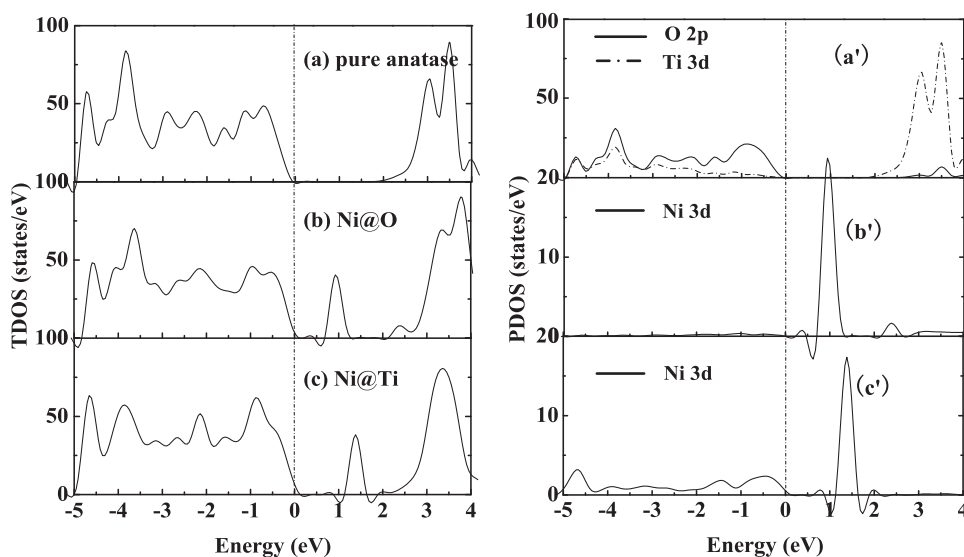**Fig. 4.** Total density of states (TDOS) and partial density of states (PDOS) for anatase supercell ($Ti_{16}O_{32}$): (a, a′) pure anatase TiO_2, (b, b′) Ni-doped (Ni@O), and (c, c′) Ni-doped (Ni@Ti). The top of the valence band of pure anatase is taken as the reference level.

3.2. Electronic properties

In order to analyze the electronic properties of Ni-doped anatase and rutile TiO_2, the calculated energy band structures of the models are shown in Fig. 3. We set the same k-points mesh to sample the first Brillouin zone for the anatase and rutile models, respectively, which is to conveniently compare the electronic structures of models. The top of the valence band of pure anatase and rutile TiO_2 are taken as the reference level. As previous density functional theory (DFT) calculations employing GGA functional [27,28], our calculated band gap of pure anatase and rutile at Γ point (Gamma point) is about 2.05 eV and 1.80 eV, respectively, smaller than the experimental value (3.2 eV for anatase structure and 3.0 eV for rutile structure) due to the well-known shortcoming of exchange-change functional. Our theoretical results are consistent with the previous study of Yang et al. (2.2 eV for anatase and 1.9 eV for rutile) [8]. However, DFT is still a widely accepted method to depict the defect states in the electronic structure calculations, and this gives reasonable explanation for the experimental results because only the relative positions of the occupied states and empty states need taking into account [27,29–31].

In Ni-doped anatase TiO_2 (Ni@O) (see Fig. 3(b)), a series of impurity energy levels (Ni 3d orbital) appear in the forbidden gap, and all of impurity energy levels are located above the valence band

maximum (VBM) and below the conduction band minimum (CBM). The host band gap is about 2.15 eV and increased by 0.1 eV versus the pure anatase case. However, the excitation energies from the occupied states above the VBM to CBM should be much smaller than the optical absorption energy of pure anatase TiO_2, which can explain why Ni-doped TiO_2 has better visible-light photocatalytic activity and a red-shift of optical absorption compared to pure TiO_2 reported in the experiment [19,20]. For Ni-doped anatase TiO_2 (Ni@Ti) (see Fig. 3(c)), two isolated states are located above the VBM and the resultant band gap is 2.0 eV. As consequence, the electron transition from these isolated states to the conduction band would lead to an obvious reduction of absorption energy, which also gives a good explanation for the experimentally observed red-shift of the absorption edge. These results are consistent with the experimental observations of Tseng et al. [19] and Nakhate et al. [20]. For pure rutile TiO_2, Fig. 3(d) shows that the calculated band gap is 1.8 eV. For Ni-doped rutile TiO_2 (Ni@O), Fig. 3(e) shows that there are two isolated energy states in the band gap of Ni@O rutile structure. This result indicates that electrons can be excited between these impurity states as well as to the host band, and thus it may improve the visible-light photocatalytic activity [19,20]. In Tseng's and Nakhate's experiments, the DRS analysis confers visible absorption edge to Ni-doped TiO_2 at 550 nm, and the XRD measurements show that samples are a mixture of anatase and rutile phases.
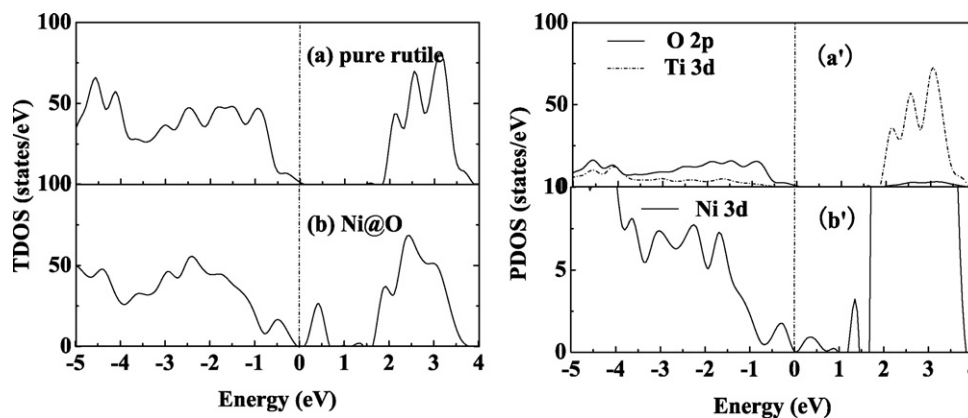

Fig. 5. Total density of states (TDOS) and Partial density of states (PDOS) for rutile supercell ($Ti_{16}O_{32}$): (a, a′) pure rutile TiO_2 and (b, b′) Ni-doped (Ni@O). The top of the valence band of pure rutile is taken as the reference level.

Hence, the shift of the optical absorption edge corresponds to a decrease of absorption energy.

To have a clear comparison, the total density of states (TDOS) and partial density of states (PDOS) of pure anatase TiO$_2$ are plotted in Fig. 4(a and a′), which indicate that the valence band mostly comprises the O 2p states while the conduction band is mostly composed of Ti 3d states. For Ni-doped (Ni@O) anatase TiO$_2$, TDOS and PDOS are also plotted in Fig. 4(b and b′), it can be observed that the band gap increases by about 0.1 eV and most Ni 3d states are located in the band gap compared with the pure anatase TiO$_2$, which may be due to stronger interactions between the Ni 3d and O 2p orbitals. Hence, the excitation from these occupied Ni 3d states to conduction band might also lead to a decrease of the photon excitation energy and induce a more significant red-shift of the absorption edge, which can possibly explain why Ni-doped TiO$_2$ has better photocatalytic activity than pure TiO$_2$ reported in experiment [19,20]. In Ni-doped (Ni@Ti) anatase TiO$_2$ (see Fig. 4(c and c′)), it is shown that the band gap has a slight decline about 0.05 eV and most Ni 3d states are located in the forbidden gap compared with the pure anatase TiO$_2$. The photon excitation energy from these occupied Ni 3d states to the conduction band can be decreased. The calculated result gives a good explanation for experimental optical absorption broadening to longer wavelength in Ni-doped TiO$_2$.

As to Ni-doped rutile TiO$_2$, our calculation of the energies of defect formation indicates that Ni impurity is preferred to substitute the O atom under both Ti-rich and O-rich growth conditions. Therefore, only configuration of Ni@O is considered in the Ni-doped rutile TiO$_2$. The TDOS and PDOS of pure and Ni-doped (Ni@O) rutile TiO$_2$ are shown in Fig. 5. The band gaps of pure and Ni-doped rutile TiO$_2$ are 1.8 eV and 1.6 eV, respectively. Several impurity levels appear in the forbidden band, which may be due to stronger interactions between the Ni 3d and O 2p orbitals. It is obvious that Ni 3d electrons have significant contribution to these impurity levels while little contribution to the valence bands and conduction bands. Hence, the excitation from these impurity levels to conduction band can lead to a decrease of the photon excitation energy and induce a significant red-shift of the absorption edge. These results give a good explanation for the experimentally observed red-shift of the absorption edge and enhanced photocatalytic activity in the visible-light range.

Consequently, Ni-doping (anatase and rutile) can lead to a decrease of the photon excitation energy, which may be responsible for the visible-light photocatalytic activity and the red-shift of optical absorption edge in Ni-doped anatase and rutile TiO$_2$. This conclusion is consistent with the experiment reported by Tseng et al. [19] and Nakhate et al. [20]. On the other hand, one should note that photocatalytic efficiency is a complex phenomenon, and experimental results are influenced by many factors, such as procedure of preparation, materials ratio, heat-treated temperatures, heat-treated times, diffusion time scales of photoexcited electron transfer from bulk to surface, and by electron–hole recombination rates. This implies that the forbidden band with impurity levels alone is not a sufficient factor to lead to high photocatalytic efficiency.

4. Conclusion

We have calculated the electronic structures of substitutionally Ni-doped anatase and rutile TiO$_2$ by means of density functional theory calculations based on plane-wave method. The calculated results indicate that substitutionally Ni to O-doped anatase and rutile TiO$_2$ have a series of impurity energy levels appearing in the forbidden gap, which may be responsible for the red-shift of

optical absorption edge and visible-light photocatalytic activity in substitutionally Ni to O-doped TiO$_2$. For substitutionally Ni to Ti-doped anatase TiO$_2$ under O-rich growth condition, Ni 3d electrons have significant contribution to these impurity levels and the band gap narrowing, which can lead to a decrease of the photon excitation energy. These results give a good explanation for the experimentally observed red-shift of the absorption edge and enhanced photocatalytic activity in the visible-light range. In addition, our calculated formation energies indicate that the synthesis of substitutionally Ni to O-doped anatase TiO$_2$ is chemically preferred under Ti-rich growth condition. Since substitutionally Ni to O-doped rutile TiO$_2$ has the lowest formation energy of all under O-rich growth condition, Ni doped rutile is overall the best host in view of visible-light excitation. Moreover, O-rich substitution is preferred over Ti-rich substitution to Ni doping of rutile TiO$_2$.

Conflict of interest statement

The authors declare that there are no conflicts of interest.

Acknowledgements

References

[1] F. Arntz, Y. Yacoby, Phys. Rev. Lett. 17 (1966) 857.
[2] M.R. Hoffmann, S.T. Martin, C. Wonyong, D.W. Bahnemann, Chem. Rev. 95 (1995) 69.
[3] H. Tang, F. Lévy, H. Berger, P.E. Schmid, Phys. Rev. B 52 (1995) 7771.
[4] H. Yamashita, M. Harada, J. Misaka, M. Takeuchi, K. Ikeue, M. Anpo, J. Photochem. Photobiol. A: Chem. 148 (2002) 257.
[5] Y.W. Wang, L.Z. Zhang, S. Li, P. Jena, J. Phys. Chem. C 113 (2009) 9210.
[6] Z. Zhou, M. Li, L. Guo, J. Phys. Chem. Solids 71 (2010) 1707.
[7] R. Jin, Z. Wu, Y. Liu, B. Jiang, H. Wang, J. Hazard. Mater. 161 (2009) 42.
[8] K. Yang, Y. Dai, B. Huang, Chem. Phys. Lett. 456 (2008) 71.
[9] W. Shi, Q. Chen, Y. Xu, D. Wu, C. Huo, Appl. Surf. Sci. 257 (2011) 3000.
[10] S. Sakthivel, H. Kisch, Angew. Chem. Int. Ed. 42 (2003) 4908.
[11] Y. Li, D.-S. Hwang, N.H. Lee, S.-J. Kim, Chem. Phys. Lett. 404 (2005) 25.
[12] Y. Choi, T. Umebayashi, M. Yoshikawa, J. Mater. Sci. 39 (2004) 1837.
[13] S.U.M. Khan, M. Al-Shahry, W.B. Ingler Jr., Science 297 (2002) 2243.
[14] G. Wu, T. Nishikawa, B. Ohtani, A. Chen, Chem. Mater. 19 (2007) 4530.
[15] S.-W. Hsu, T.-S. Yang, T.-K. Chen, M.-S. Wong, Thin Solid Films 515 (2007) 3521.
[16] H. Irie, S. Washizuka, K. Hashimoto, Thin Solid Films 510 (2006) 21.
[17] W. Zhao, W. Ma, C. Chen, J. Zhao, Z. Shuai, J. Am. Chem. Soc. 126 (2004) 4782.
[18] S.D. Sharma, D. Singh, K.K. Saini, C. Kant, V. Sharma, S.C. Jain, C.P. Sharma, Appl. Catal. A: Gen. 314 (2006) 40.
[19] H.H. Tseng, M.C. Wei, S.F. Hsiung, C.W. Chiou, Chem. Eng. J. 150 (2009) 160.
[20] G.G. Nakhate, V.S. Nikam, K.G. Kanade, S. Arbuj, B.B. Kale, J.O. Baeg, Mater. Chem. Phys. 124 (2010) 976.
[21] G. Kresse, J. Hafner, Phys. Rev. B 47 (1993) 558.
[22] J.A. White, D.M. Bird, Phys. Rev. B 50 (1994) 4954.
[23] J.P. Perdew, S. Burke, M. Ernzerhof, Phys. Rev. Lett. 77 (1996) 3865.
[24] H.J. Monkhorst, J.D. Pack, Phys. Rev. B 13 (1976) 5188.
[25] M.Y. Kuo, C.L. Chen, C.Y. Hua, H.C. Yang, P. Shen, J. Phys. Chem. B 109 (2005) 8693.
[26] R. Shirley, M. Kraft, Phys. Rev. B 81 (2010) 075111.
[27] C. DiValentin, G. Pacchioni, A. Selloni, Phys. Rev. B 70 (2004) 085116.
[28] H. Weng, J. Dong, T. Fukumura, M. Kawasaki, Y. Kawazoe, Phys. Rev. B 73 (2006) 121201.
[29] J. Lee, J. Park, J. Cho, Appl. Phys. Lett. 87 (2005) 011904.
[30] K. Yang, Y. Dai, B. Huang, J. Phys. Chem. C 111 (2007) 18985.
[31] K. Yang, Y. Dai, B. Huang, Phys. Rev. B 76 (2007) 195201.